KNOWLEDGEABLE RESEARCH (KR)
ISSN: 2583-6633 | CODEN: KRABAU
International Open-Access Peer-Reviewed Refereed Multidisciplinary Journal
https://knowledgeableresearch.com
Vol. 5, Issue 08,2026

Received: 09/07/2026 | Accepted: 26/08/2026 | Published: 30/08/2026

Numerical Analysis of Gas Flow around Muzzle with Rotary Brake

Im Chol, Kim Gum Song, *Kim Un Il, Han Yong Gil, Ju Nam Il and Choe Yong Su

Faculty of Mechanical Engineering, Kim Chaek University of Technology, Pyongyang, DPR Korea

Abstract

The muzzle brake is intended to decrease recoil force of gun and in the past, the main attention has been paid to increase the efficiency in designing muzzle brakes. In this paper, in order to improve its efficiency, we suggest an innovative approach for blocking axis-directional flow of propellant gas by rotary brake after the projectile exits the muzzle. We establish the unsteady three-dimensional CFD simulation approach based on AUSM+ scheme for estimating the action characteristics of rotary brake and its effectiveness of muzzle brake. Through CFD simulation, we confirm that rotary brake acts safely without interference of projectile, and analyze the flow field around muzzle and determine the efficiency of newly-suggested muzzle device. By comparing our simulation result with test data, we prove the accuracy of simulation approach used here. Thus, this shows that it is possible to increase greatly its efficiency by installing rotary brake in muzzle

Keywords: *Rotary brake, Muzzle brake, Muzzle flow field, Efficiency, Numerical simulation*

***Corresponding Author:**
Kim Un Il
Email: UI.KIM72@star-co.net.kp

1.Introduction

It is necessary for a gun designer to estimate exactly the flow field around the muzzle, for designing a proper muzzle brake. In general, after the base of projectile escapes from the muzzle, the propellant gas with high temperature and high pressure emits into the atmosphere, and it can cause many undesirable phenomena such as blast waves, acoustic waves, pressure waves, electromagnetic radiation, muzzle flash, and smoke [1].

An air column driven out of the barrel ahead of the projectile also generates a precursor flow field, which makes the muzzle flow more complex due to the blast shock of precursor gas [1, 2].

In addition, at the moment of firing, it is well known to cause many complicated, peculiar phenomena around muzzle because of high-strength overpressure, high-temperature and high-velocity gas flow.

This happens only at domain not far from muzzle (less than 100 times of muzzle diameter). This flow field around muzzle involves phenomena such as the expansion wave, shock wave, shear-layer and explosive wave.

These phenomena, which cause at the gun firing, can consider as the combination of lots of acoustic waves from a result of the following four-main components. In other words, they are the muzzle blast waves by propellant gas flowing at supersonic velocity, the shock waves induced by supersonic projectile motion, the compression waves formed by air-column ahead of projectile in the barrel, the acoustic waves by collision of weapon-parts during firing and so on [1-3].

Herein, the components which have effects on the recoil force of gun are the precursor compression waves and blast waves by air-column ahead of the projectile, and various shock waves by interaction between the projectile and air-propellant gas.

However, as the flow field around muzzle forms and changes in a very short time (less than a few ms), it is very difficult to analyze its field exactly by any experimental methods. Thus, in the past, many attempts have been tried for analyzing the flow field around muzzle by using CFD numerical simulation.

Xiaohai Jiang solved the Arbitrary Lagrangian–Eulerian (ALE) of Euler equations by using the AUSMDV scheme on the dynamic chimera grid, and discussed in detail the prominent characteristics including the propagation of first and second blast waves and the generation of bow shock based on the numerical results [2].

Changfei Zhuo simulated the muzzle flow with a base bleed projectile and a gun-launched missile based on dynamic overlapped grids approach [4, 5]. In this simulation, a high-resolution upwind scheme (AUSMPW+) and detailed reaction kinetics model were employed to solve the chemical non-equilibrium Euler equations and then the development process of muzzle flows with base bleed projectile and the rapid depressurization process in the combustion chamber of base bleed unit were analyzed in detail.

Qiongyao Qin simulated the precursor flow generated by the precursor gas driven out of the barrel ahead of the projectile and the development of muzzle flow with chemical reaction based on an inert gas labeling method [1]. It was demonstrated from the results that the secondary temperature rise in the intermediate region behind the Mach disk was attributed to combustion in this area. A high-resolution upwind scheme, AUSM+ (Advection Upstream Splitting Method), and detailed reaction kinetics model were employed to solve the multispecies Navier–Stokes equations with finite rate chemistry.

Ye Luo investigated the blast flow field around muzzle in correlation with the projectile nose shapes of flat-nosed, cone-nosed, and blunt-nosed projectiles [6].

In the numerical simulations mentioned above, the precursor flow was considered as concluded by Schmidt [7] and Wei Lu [8], but such simulations were based on a simple two-dimensional axisymmetric model.

In addition, many studies were conducted to determine the muzzle brake efficiency based on the blast flow field around muzzle.

Numerical investigations of the projectile launch process with different muzzle brakes have been performed by Huanhao Zhang [9] with both two- and three-dimensional unsteady Euler equations and hybrid Roe type scheme. The efficiency of the three-way muzzle brake was calculated, which was also comparable to the corresponding experimental value.

Hongxia Lei analyzed the forces acted on the muzzle with several side-blowholes through 3D CFD simulation and estimated the muzzle brake efficiency [10].

Sherif Said carried out design optimization of muzzle brake for sniper rifle by using an analytical model for calculating muzzle brake efficiency and weapon recoil force [11].

These studies will also be helpful for understanding the complex phenomena involved while the projectile escapes from the muzzle.

But most of them assumed the physical model of muzzle to be a simple two-dimensional axisymmetric, or even for three-dimensional model, they had studied only the typical fixed-structure.

Therefore, we suggest a new muzzle-device with rotary brake in this paper, and we are going to estimate the performance and effectiveness of muzzle device designed by using the unsteady computational fluid dynamic (CFD) simulation.

The typical schematic of shock waves is schematically shown in Fig.1, which form by the precursor flow field and interaction of the projectile (escaped from barrel), gas and air.

After escaping of the projectile from barrel, the flow of the main propellant gases starts to exhaust.

Because the propellant gas usually exhausts from the barrel with pressure ratio more than 500, the precursor blast wave is very quickly generated. The incident shock formed in muzzle terminates in the triple point, from which the reflected shock wave and Mach disk originate.

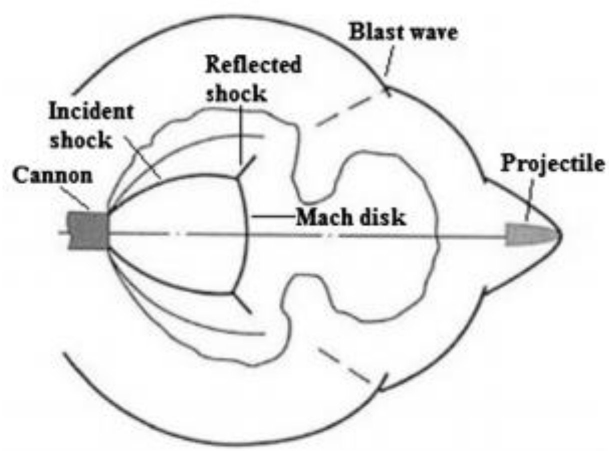

Figure 1. Typical schematic of flow-field around muzzle flows by moving projectile

2.Numerical Techniques

2.1. Computational Model

In order to decrease the recoil force of the gun, the structure of the newly designed muzzle device is given in Fig.2.

By installing the rotary brake on the muzzle device, it rotates around its rotary axis under the effect of gas pressure after escaping of projectile, and then, as a result, it is supposed to block the front blowhole through which the projectile has just exited.

Therefore, it is able to increase the efficiency of muzzle device because the gas-escaping passages which consist of three blow holes will be changed into two blowholes, and then increase the front direction gas force acted on the muzzle brake.

The rotary brake is designed to rotate back to its original position by the action of the gravitational force or the reaction force of torsion spring when gas exhausting is terminated and the force moment of propellant gas acted on rotary brake is diminished.

The projectile diameter and inner diameter of the barrel are both 14.5mm and the length of barrel bore is 1280mm long.

The projectile mass is 80grams and the propellant 30grams.

As shown in computational model, the rotary brake as well as the projectile will be in motion during firing. The computational domain set up for CFD simulating of muzzle device is shown in Fig.3.

In order to estimate the performance of muzzle device exactly, the simulation must be implemented from the first moment when the projectile starts to move in barrel to the final moment of aftereffect period, and the force acted on the muzzle device must be calculated at each time step.

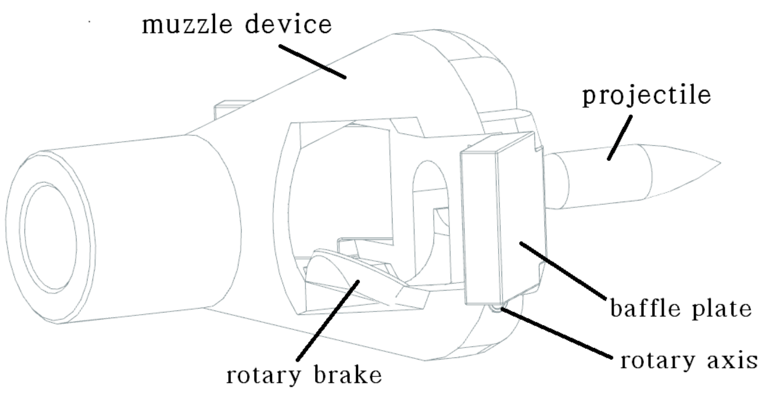

Figure 2. Structure of muzzle device with rotary brake

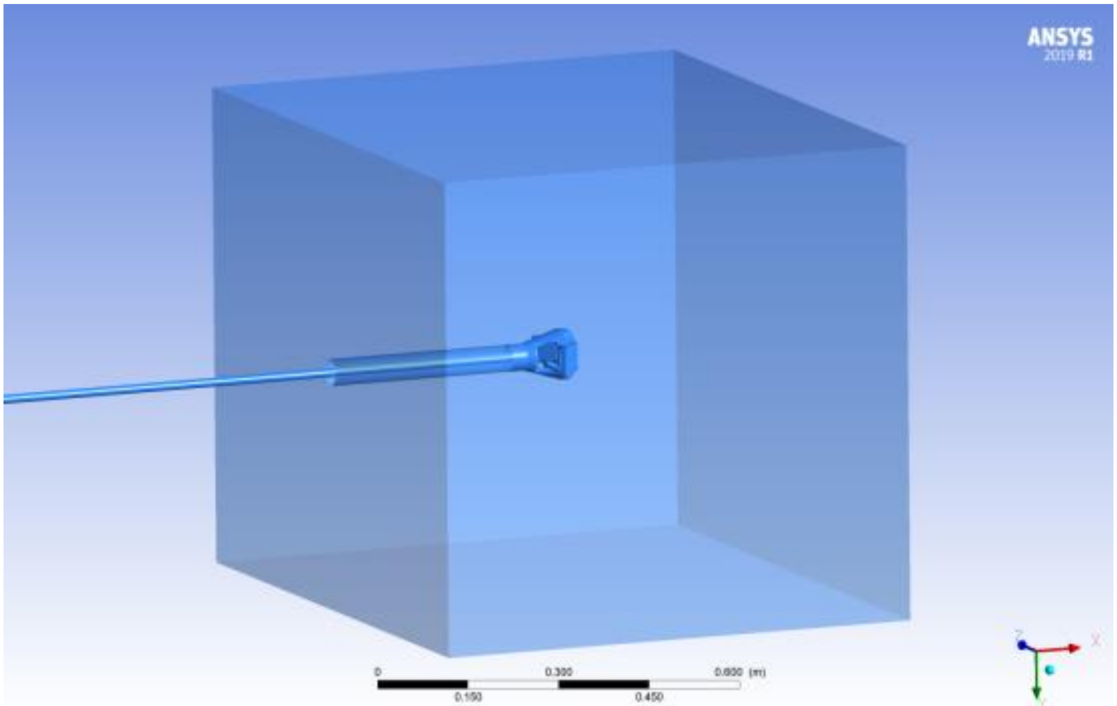

Figure 3. Computational domain to simulate the muzzle brake

2.2. Numerical Method

For simulating the firing process under the condition relatively similar to practical situation, CFD numerical simulation to get the efficiency of the muzzle brake is conducted by the following four-periods from the viewpoint of mesh generation.

The first period is the duration when the projectile moves inside barrel (interior ballistics period).

The second period is the aftereffect period when the projectile interacts with the propellant gas flow after escaping from barrel.

The third period is the aftereffect period when the rotary brake is closed.

Finally, the fourth period is the aftereffect period after the rotary brake is closed.

In the first period, the projectile in the initial position of barrel bottom is accelerated under the effect of extremely high pressure of propellant gas behind that. The interior ballistics equations of two-phase flow according to the charge-burning law are solved by using the dispersion-controlled dissipative(DCD) scheme. After obtaining the propellant gas-state parameters such as the gas generation rate, pressure and temperature, the precursor flow is considered by using these input conditions, reproducing the projectile motion in gun bore.

The projectile motion follows Newton's law.

The friction between the projectile and the inside surface of bore is ignored in this case.

The input parameters prescribed at the combustion chamber and the projectile motion are performed through UDF.

For simulating analysis of the first period, the dynamic mesh approach is applied by using the dynamic layering method.

Herein, for preserving the mesh refinement around the projectile, it is necessary to set the generating-zone and destroying-zone of the dynamic mesh layer into combustion chamber bottom boundary and far-field boundary, respectively. It allows for the fluid zone including projectile to conduct one dimensional motion on the basis of force acting on front and rear walls of projectile.

It will be able to improve the precision in capturing the precursor compressive wave ahead of the projectile.

In addition, the dynamic remeshing method is applied in the final part of the first period, in which the air column ahead of projectile has an effect on the rotary brake.

In the second period, the projectile still takes in translational motion and the rotary brake takes in rotary motion at the same time because a torque acts on the rotary brake from effects of pressure wave by air column ahead of projectile. It is possible to model the translational motion of projectile and the rotary motion of brake together by using the six-degree of free (6DOF) solver of Ansys Fluent. Wherein, we set the motion zone around muzzle apart, and apply the remeshing method to that.

Because of the rapid expansion of propellant gas after the projectile exits the barrel, the dynamic mesh adaption is adopted according to the gas parameters in order to consider the generation of blast waves around muzzle.

If the projectile is a certain distance away after exiting the muzzle, the blast wave formed by projectile will be considered not to affect the flow field around the muzzle because of high speed of the projectile. From this moment, analysis of the projectile motion may be cancelled because that is an insignificant work on flow computation around the muzzle and it is able to efficiently decrease the cost of computation.

In this paper, when the projectile moves one meter away from the muzzle device, we consider that the second period finishes.

In the third period, the projectile moves away enough and does not have any effect upon flow field around muzzle. Hence, we remove the projectile zone from the computational domain without analyzing the projectile motion and simulate only the rotary motion of rotary brake by using the dynamic remeshing method.

The motion of rotary brake during the third period is computed with six DOF solver of Fluent.

The unsteady dynamic mesh adaption method is still applied to improve the correctness of flow-parameter estimation in the third period.

In the fourth period, there is no dynamic mesh variation and so flow variables are changed in the stationary flow domain and the pressure inside barrel decreases with time. Therefore, the computation during the fourth period is performed in the same way as that of general unsteady CFD computation in which the initial conditions are setup with flow parameters at the final moment for the third period.

Whenever transmitting from the first period to the fourth period, the mesh replacement is applied. The mesh replacement is composed of interpolating the solved-data based on the mesh of the former-period into the new–period mesh according to least squares interpolation method.

During the mesh replacement, the parameter values of flow field remain original at the final moment of the prior period. Hence, it is possible to succeed the computation data of the prior period within the replaced mesh of new period.

It ensures the continuous flow progression from the time when the projectile starts to move inside barrel to the final moment of aftereffect periods. Fig.4 shows the meshes around the muzzle used from the first to the fourth periods.

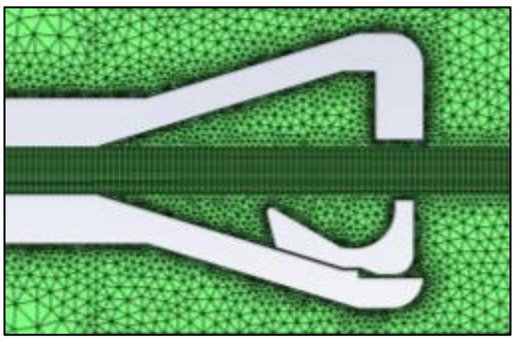

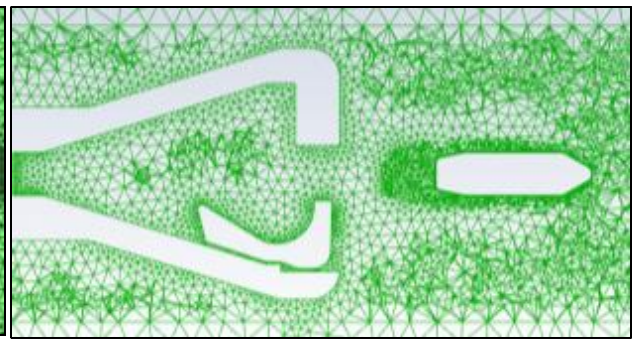

(a) the first period **(b) the second period**

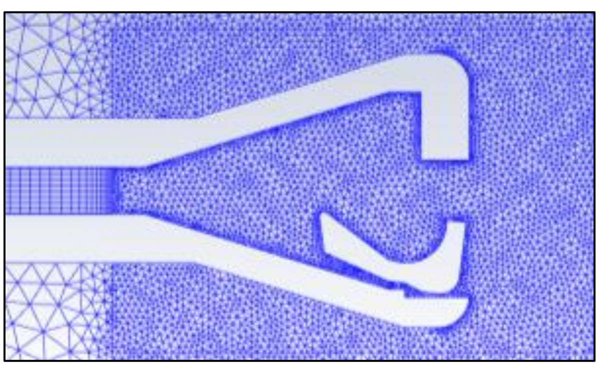

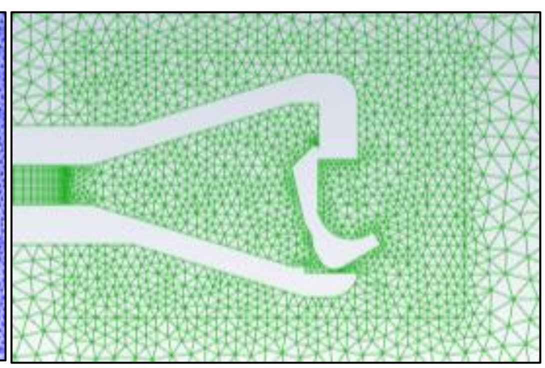

(c) the third period **(d) the fourth period**

Figure 4. Meshes around muzzle used for simulation analysis in all periods

2.3. Governing equations

The CFD computations during the first period are based upon SST k-ω turbulence model and the Navier-Stokes equations.

From the second period to the fourth period, The Reynolds number of flow based on muzzle diameter is $Re = \frac{\rho v d}{\mu} \approx 10^7 \sim 10^8$, so the effect of viscous force relative to pressure force can be ignored.

Therefore, it is reasonable to perform the inviscid flow analysis based on the Euler equations in these stages.

For this reason, the effects of viscosity and chemical reaction are negligible in current study.

Considering these assumptions, for an ideal gas, the time-dependent Arbitrary Lagrangian–Eulerian (ALE) equations of the conservation system in a general deformation control volume $\Omega(t)$ can be expressed as;

$$\frac{\partial}{\partial t}\iiint_{\Omega(t)} \mathbf{Q} d\Omega + \oiint_{S(t)} (\mathbf{F} - \mathbf{Q}\boldsymbol{\omega}) \cdot \mathbf{n} ds = 0$$

(1)

where, $\mathbf{Q} = [\rho,\ \rho V,\ \rho E_t,\ \rho f_i]^T$, $\mathbf{F} = \mathbf{QV} + \mathbf{G}$, $\mathbf{G} = [0,\ p\mathbf{I},\ p\mathbf{V}]^T$.

ρ, p are the density and pressure, respectively, $\mathbf{v}$ is the velocity vector of fluid, E_t is total energy per unit mass, and f_i is mass percentage of the i th component.

$S(t)$ is the surface which encloses the time-dependent control volume $\Omega(t)$, and n is the outward unit vector normal to the boundary $S(t)$.

I is the unit tensor, and $\boldsymbol{\omega}$ denotes the surface velocity of the time-dependent control volume $\Omega(t)$.

The numerical scheme employed is a finite-volume, Riemann solver and the second-order upwind scheme is applied to estimate the spatial derivative term.

The temporal derivative term is estimated by the implicit time stepping method, that is, the dual-time formulation, and a pseudo-time-derivative term is introduced to it. Then, the Eq.(1) can be written as follows;

$$\frac{\partial}{\partial t}\iiint_{\Omega(t)} \mathbf{Q} d\Omega + \Gamma \frac{\partial}{\partial \tau}\iiint_{\Omega(t)} \mathbf{Q} dV + \oiint_{S(t)} (\mathbf{F} - \mathbf{Q}w) \cdot n ds = 0$$

(2)

where, t denotes a real physical-time, and τ is a pseudo-time used in the time-marching procedure.

Note that the second term vanishes gradually according to $\tau \to \infty$ on the left side of Eq. (2) and it is equal to Eq. (1).

In the Eq.(1), the convective flux vector F is computed based on high-resolution AUSM+ scheme.

A classical Roe flux difference splitting solver usually fails on very strong expansions [12]. AUSM+ scheme provides exact resolution of shock and contact discontinuities.

2.4. AUSM+ Scheme

During spatial discretization process, it is necessary to estimate the quantity of F crossing the boundary *S(t).*

In the present study, the inviscid flux is computed by the AUSM+ scheme [13, 14].

In this scheme, the inviscid flux F is splitted into a convection flux term and a pressure flux term.

$$\mathbf{F} = \mathbf{F}_C + \mathbf{F}_p \tag{3}$$

where,

$$\mathbf{F}_C = M \cdot a \cdot \mathbf{Q} \tag{4}$$

$$\mathbf{F}_p = (0, p, p, 0)^T \tag{5}$$

where, $H = e + p/\rho$ is the enthalpy.

From the expressions above, it can be seen that the convection term contains the Mach number *M*, the local sound velocity a and the flow parameter Q, whereas the pressure term contains only the pressure *p*. The flux across the boundary can be written;

$$\mathbf{F}^C_{1/2} = M_{1/2} \cdot a_{1/2} \cdot \mathbf{Q}_{1/2} \tag{6}$$

$$\mathbf{F}^p_{1/2} = (0, p_{1/2}, p_{1/2}, 0)^T \tag{7}$$

According to the flow direction at the boundary, the flow parameter Q is possible to obtain from the controlling-volumes on both side boundaries.

$$\mathbf{Q}_{1/2} = \begin{cases} \mathbf{Q}_L & M_{1/2} \geq 0 \\ \mathbf{Q}_R & M_{1/2} < 0 \end{cases} \tag{8}$$

Considering that Mach number M is affected by this characteristic wave, the splitting function is used in calculating Mach number at the boundary.

$$M^{\pm} = \begin{cases} \frac{1}{2}(M \pm |M|) & |M| \geq 1 \\ \pm\frac{1}{4}(M \pm 1)^2 \pm \frac{1}{8}(M^2 - 1)^2 & |M| < 1 \end{cases} \tag{9}$$

The pressure splitting function can be written;

$$p^{\pm} = \begin{cases} \frac{1}{2}(1 \pm sign(M)) & |M| \geq 1 \\ \pm\frac{1}{4}(M \pm 1)^2(2 \mp M) \pm \frac{3}{16}M(M^2 - 1)^2 & |M| < 1 \end{cases} \tag{10}$$

A method for calculating the local sound velocity also has an effect on the computational accuracy. In order to guarantee the accuracy of capturing shock wave, the local sound velocity at the boundary is computed with the sound velocities of both sides considered. The expression is as follows:

$$a_{1/2} = \begin{cases} (a^*_{1/2})^2 / u_L & |u_L| \geq a^* \\ \min(\hat{a}_L, \hat{a}_R) & |u_L| < a^* \end{cases} \tag{11}$$

In the AUSM+ scheme, the numerical flux is computed by dividing into the convection and pressure terms as above, so it avoids using an explicit artificial dissipation.

3. Results and Discussion

Fig. 3 and 4 show the Mach number contours around the muzzle at different moments after escaping of projectile from barrel. After the high-pressure propellant gases escapes from the muzzle, it reaches rapidly at an acoustic condition in muzzle device and transmits the inner energy into the kinetic energy. At this moment, the moving velocities of the propellant gases reach about Mach 4.5. As shown on Fig. 3 a), it can be seen that the flow field around muzzle has the asymmetry in longitudinal section, due to the rotary brake and it causes to act as a disturbance factor on the projectile but only in longitudinal section. At t=0.2ms after the start of aftereffect period, the different shock wave fields formed around muzzle and the corresponding gas-air phase distributions are shown in Fig. 5. At this moment, it is clear that the shock in gas phase and the blast wave in air phase are formed through three directions because of rapid expansion of propellant gases. And the incident shock, Mach disc, and reflected shock were captured clearly from three directions, respectively. Referring to Fig. 1, the estimation of flow field obtained can be considered to be proper. Comparing Fig. 5 b) with Fig. 7 (a), the bow shock is formed at t=0.17ms due to the effect of projectile tail, while the Mach disc is formed at t=0.2ms, as the projectile moves forwards.

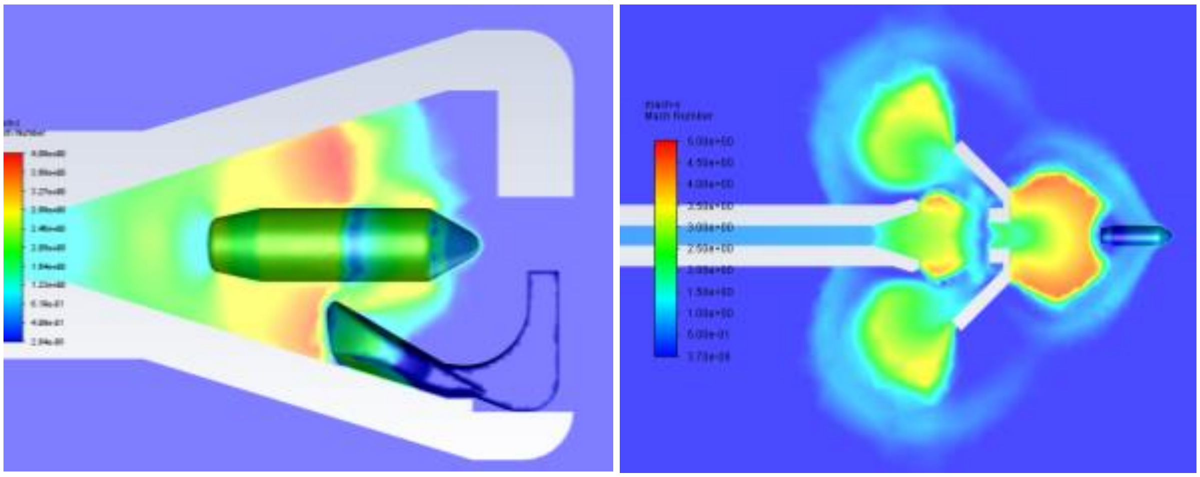

(a) longitudinal-section at t=0.04ms **(b) transverse section at t=0.17ms**

Figure 5. Mach number contour at several moments of the 2nd period

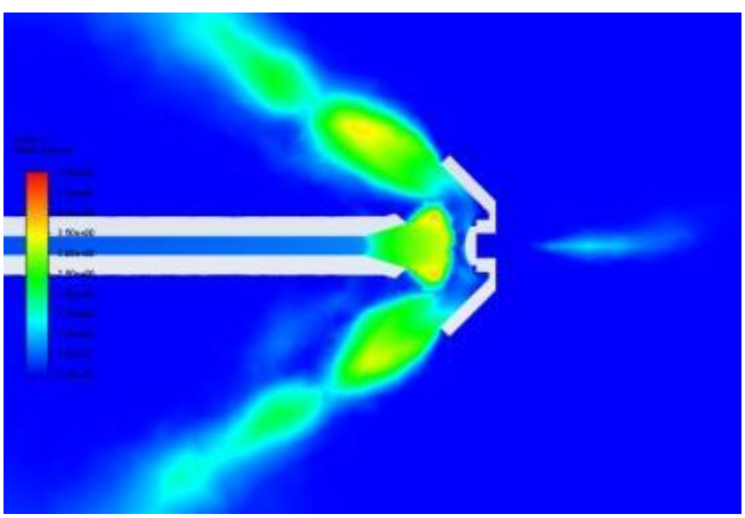

Figure 6. Mach number contour of transverse section at t=5ms of the 4th period

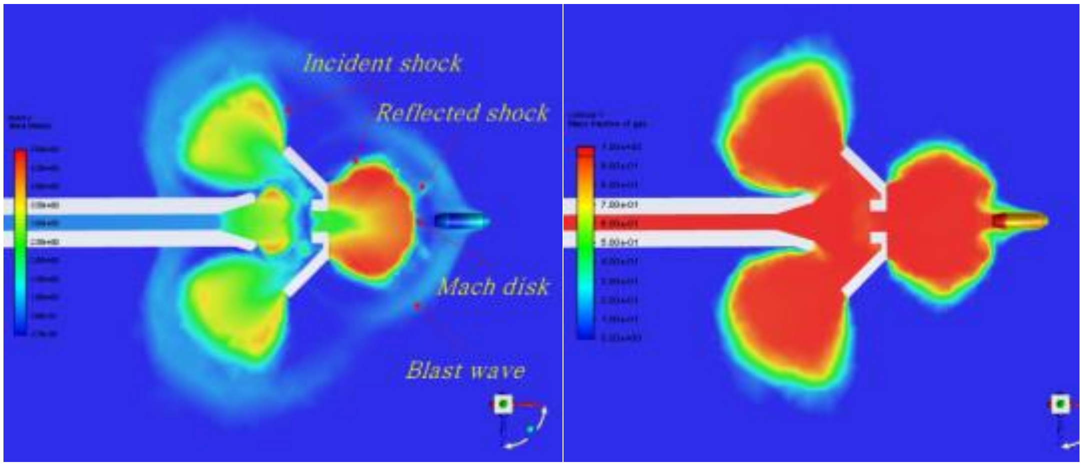

(a) ***Mach number*** **(b)** ***gas-phase***

Figure 7. Contours of Mach number and gas-phase at t=0.2ms

As a result of CFD simulation for the muzzle device with rotary brake, the flow-time according to each period is obtained as follows;

The first period is 0~2.5ms and the second 2.5~2.73ms and the third 2.73~3.7ms and the fourth 3.7~16.4ms.

The projectile escapes completely from the muzzle device at 0.1ms after the start of aftereffect period. In other words, the projectile escapes from the muzzle at 2.6ms after the start of motion. At the same time, the rotary brake starts to rotate with the effect of torque by means of the precursor air flow and the propellant gas flow followed, but its angle of rotation can be negligible (less than 0.1 degree). This implies that the rotary brake behaves safely without the collision with the projectile during firing.

The rotary brake terminates the rotating and blocks the muzzle at 3.7ms.

After that a positive moment of propellant gas is exerted on the rotary brake all the time until the final moment of the fourth period and it ensures that the rotary brake has the ability to increase the efficiency of muzzle brake by blocking the propellant gases efficiently without the collision with the projectile.

It can be known that the aftereffect time (when the average barrel pressure is less than 0.2MPa) 16.4ms will be longer due to the effect of muzzle device compared with that (10ms) in the absence of muzzle device.

In Fig. 6, the variable curves of barrel pressure and recoil force indicate comparatively in the presence or in the absence of muzzle device.

As shown in Fig. 6 a), the barrel pressure decreases slowly in the presence of muzzle device than in the absence of it after the end of the first period.

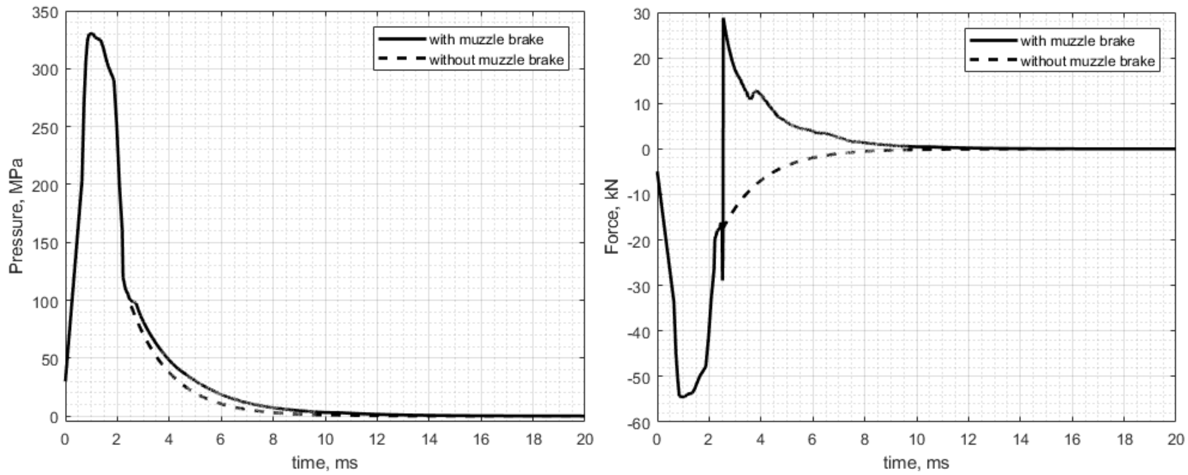

(a) barrel pressure **(b) x-directional force (negative recoil force)**

Figure 8. Variable characteristics of barrel pressure and recoil force according to time, with and without muzzle brake

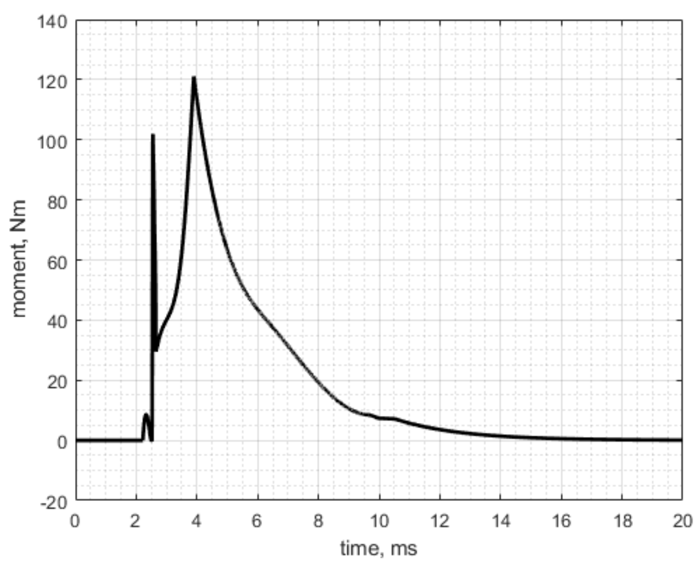

Figure 9. Variable torque characteristics of rotary brake with time

In the Fig. 6 b), the recoil force of gun increases with starting of the second period because of action of gas pressure on the muzzle cone, and at the moment of t=2.54ms, x-directional force converts abruptly into the positive value, while the gas with a high energy acts on the rotary brake and baffle.

Next, x-directional force decreases with time, and then, with closing of rotary brake, it increases a little again, because the area of supporting gas force increases. After that, it decreases exponentially with time.

Fig. 7 shows the variable characteristics of torque acting on rotary brake.

As a result of simulation, the torque of gas which acts on rotary brake, at the final moment of aftereffect period, is $M_{\text{gas}} = 0.4\ \text{Nm}$, and it is greater than the gravitational moment of brake $M_{\text{g}} = 0.0215\ \text{Nm}$.

This confirms that the brake will not be opened again until the final moment of aftereffect period.

To verify the accuracy of the simulation, the efficiency of muzzle brake is calculated by using the efficiency calculating formula, which can be expressed as

$$\eta = \frac{E_0 - E_1}{E_0} \times 100\% = (1 - \frac{M_1}{M_0}\frac{V_1^2}{V_0^2}) \times 100\ \% \tag{12}$$

where the subscript label 0 and 1 represent without and with the muzzle brake. M is the mass of recoiling parts and V is the free recoil velocity of the barrel at the start of the aftereffect period.

Computational results reveal that the efficiency of muzzle device with rotary brake is 68.6%, which is close to the experimental result (64.8%). The error is 3.8% and this implies that the computational assumptions for unsteady flow simulation and the computation method are reasonable.

4. Conclusion

In this paper, we suggested the muzzle device with rotary brake. Numerical simulation of a muzzle brake flow field based on unsteady CFD technology was conducted concerning the muzzle with rotary brake, and the results of this study show the following conclusions.

(i) During the projectile firing, the rotary brake starts to rotate with the effect of torque by means of the precursor air flow and the propellant gas flow, but its rotation position is a very close approximation to its initial position (less than 0.1 degree) until the moment when the projectile exits completely the muzzle device. So the rotary brake blocks the gas flow safely without collision with the projectile. The blocking action of rotary brake continues until end of aftereffect period, decreases the recoil force of the gun efficiently and increases the muzzle brake efficiency greatly.

(ii) The aftereffect time in case of muzzle with rotary brake will be longer compared with that in absence of muzzle.

(iii) The flow field around projectile has the asymmetry in longitudinal section when the projectile moves inside the muzzle device, due to the asymmetry of muzzle brake structure and it may cause to act as a disturbance factor on the projectile but only in longitudinal section.

This study can provide the possibility to increase muzzle brake efficiency greatly by installing a simple rotary brake and provide the methodology for designing the efficient muzzle brake by using CFD.

Acknowledgment

The authors would like to thanks Prof. Dr. Kim Song Hyok, Ryang Myong Il and Kim Jo Hyok teachers who gave valuable guidance to the writing of the paper.

Funding
This work was partially supported by Kim Chaek University of Technology
Conflicts of Interest

The authors declare no conflicts of interest.

References

[1] Qiongyao Qin and Xiaobing Zhang, Numerical investigation on combustion in muzzle flows using an inert gas labeling method, *Int. J. Heat. Mass. Trans.,* 2016, 101, 91-103

[2] X.H. Jiang, Z.H. Chen, B.C. Fan, H.Z. Li, Numerical simulation of blast flow fields induced by a high-speed projectile, Shock Waves, 2008, 18:205-212

[3] Y. Dayan and D. Touati, Simulation of unsteady muzzle flow of a small-caliber gun, Advances in Fluid Mechanics VI, 2006, 165-171

[4] C.F. Zhuo, X.S. Wu, F. Feng, Q. Liu, H. Ma, Numerical simulation of the muzzle flows with base bleed projectile based on dynamic overlapped grids, *Comput. Fluids,* 2014, 105, 307-320

[5] C.F. Zhuo, F. Feng, X.S. Wu, Development process of muzzle flows including a gun-launched missile, *Chinese J. Aeronaut.,* 2015, 28(2), 385-393

[6] Ye Luo, Da Xu, Hua Li, Analysis of the Dynamic Characteristics of the Muzzle Flow Field and investigation of the Influence of Projectile Nose Shape, *Appl. Sci.,* 2020, 10, 1468, doi: 10.3390/app10041468

[7] E.M. Schmidt, R.E. Gordnier, K.S. Fansler, Interaction of gun exhaust flowfields, *AIAA J.,* 1984, 22 (4), 516–517.

[8] Wei Yu, Xiaobing Zhang, Aerodynamic Analysis of Projectile in Gun System Firing Process, *J. Appl. Mech. T ASME,* 2010, 77, 051406

[9] Huanhao Zhang, Zhihua Chen, Xiaohai Jiang, Hongzhi Li, Investigations on the exterior flow field and the efficiency of the muzzle brake, *J. Mech. Sci. Technol*., 2013, 27, 95-101, doi:10.1007/s12206-012-1223-8

[10] H.X. Lei, Z.J. Wang, J.L. Zhao, Stress Analysis of Muzzle Brake by Using Fluid-Solid Coupled Method, *J. Eng. Sci. Technol. Rev.,* 2016, 9(4) 48-55

[11] M. Sherif Said, Ossama R. Abdelsalam, Mohamed H. Aboul, Design Optimisation of Muzzle Brake for Sniper Rifle, *Def. Sci. J.,* 2018, 68(5), 438-444, doi : 10.14429/dsj.68.12754

[12] Roxan Cayzac, Eric Carette, Computational Fluid Dynamics and Experimental Validations of the Direct Coupling Between Interior, Intermediate and Exterior Ballistics Using the Euler Equations*, J. Appl. Mech. T ASME,* 2011, 78, 061006

[13] M.S.Liou, A Sequel to AUSM: AUSM+, *J. Comput. Phys.,* 1996, 129(2), 364-382.

[14] S. Phongthanapanich, A modified multidimensional dissipation technique for AUSM + on triangular grids, *Int. J. Comut. Fluid. D.,* 2015, 29, 1-11